Quantitative Modeling of Chloride Conductance in Yeast TRK Potassium Transporters

Alberto Rivetta,* Clifford Slayman,* and Teruo Kuroda†
*Department of Cellular and Molecular Physiology, Yale School of Medicine, New Haven, Connecticut; and †Department of Genomics and Applied Microbiology, Graduate School of Medicine, Dentistry and Pharmaceutical Sciences, Okayama University, Okayama, Japan

ABSTRACT So-called TRK proteins are responsible for active accumulation of potassium in plants, fungi, and bacteria. A pair of these proteins in the plasma membrane of *Saccharomyces cerevisiae*, ScTrk1p and ScTrk2p, also admit large, adventitious, chloride currents during patch-recording (Cl^- efflux). Resulting steady-state current-voltage curves can be described by two simple kinetic models, most interestingly, voltage-driven channeling of ions through a pair of activation-energy barriers that lie within the membrane dielectric, near the inner (α) and outer (β) surfaces. Two barrier heights (E_α and E_β) and two relative distances (a_1 and b_2) from the surfaces specify the model. Measured current amplitude parallels intracellular chloride concentration and is strongly enhanced by acidic extracellular pH. The former implies an exponential variation of a_1, between ~0.2 and ~0.4 of the membrane thickness, whereas the latter implies a linear variation of E_β, by 0.69 Kcal mol^{-1}/pH. The model requires membrane slope conductance to rise exponentially with increasingly large negative membrane voltage, as verified by data from a few yeast spheroplasts that tolerated voltage clamping at −200 to −300 mV. The behaviors of E_β and a_1 accord qualitatively with a hypothetical structural model for fungal TRK proteins, suggesting that chloride ions flow through a central pore formed by symmetric aggregation of four TRK monomers.

INTRODUCTION

Accessory, or adventitious, channel-like ion fluxes have been widely observed in ion-coupled amine transporters and excitatory amino-acid transporters from neural tissues of vertebrates and from a variety of invertebrates (1–4). Such movements either can be triggered by application of the substrate (but occur in non-stoichiometric quantities, i.e., transport-associated currents), or can arise under special conditions in the absence of substrate (constitutive leakage currents). In different transporter systems, these accessory fluxes comprise mainly chloride ions or sodium ions, but the question of whether they parasitize the normal transport pathway, as, e.g., in multi-ion single-file transit (5,6), or follow a completely different route (7), is still unclear.

The best understood of these transporters possess several peptide loops which enter and re-exit the cell membrane from one side, as judged initially from hydrophobicity calculations and accessibility measurements (8,9) and confirmed recently in crystal structures (10). Such recurrent loops (*P*)—sandwiched between bona fide transmembrane helices (*M*)—are now widely recognized as signature features of ion channels, and are best characterized in potassium channels, especially the crystallized bacterial potassium channel, KcsA from *Streptomyces lividans* (11,12). The finding of potassium-channel-like recurrent-loop sequences in the TRK family of microbial and plant active K^+ transporters (13–15), led to the demonstration that those sequences could be folded like K^+ channels, overlaid upon the crystal structure of KcsA (16). Recent experimental work (both functional and topological) on several different species of TRK proteins has verified the structural inference, specifically the presence of four MPM motifs within the complete folded structure of TRK proteins (17–21), as illustrated in Fig. 1.

Two members of the TRK family, ScTrk1p and ScTrk2p, are present in the yeast *Saccharomyces cerevisiae*, and these have recently also demonstrated large inward currents which are dependent upon intracellular chloride concentration (22). In wild-type yeast grown in abundant potassium, and assayed by conventional patch-clamping, the putative chloride currents are approximately equal in size through the two proteins, Trk1p and Trk2p, but the total amplitude is modulated by both strain background and cell size. The kinetic behavior of these currents—their overall current-voltage relationship—resembles that of the mammalian glutamate transporter EAAT5 (3) expressed in *Xenopus* oocytes, but chloride flux in the yeast TRK proteins may occlude the proteins' normal potassium-transport function (22). It is certainly not initiated by the potassium transport process.

Although a variety of essentially artifactual modes have been suggested for passage of chloride through biological membranes (23–27), these spurious modes can be ruled out for the TRK proteins, by observations already presented (22). Principally, it is clear that generalized membrane effects of chloride are not involved, because deletion of both of the yeast TRK proteins eliminates >90% of the chloride-dependent currents, and only elevated intracellular chloride evokes the currents (inward, reflecting chloride efflux), whereas elevated extracellular chloride evokes no corresponding currents (outward). Furthermore, as is demonstrated

Submitted May 17, 2005, and accepted for publication July 6, 2005.

Address reprint requests to C. L. Slayman, Tel.: 203-785-4478; Fax: 203-785-5535; E-mail: clifford.slayman@yale.edu.

0006-3495/05/10/2412/15 $2.00

doi: 10.1529/biophysj.105.066712

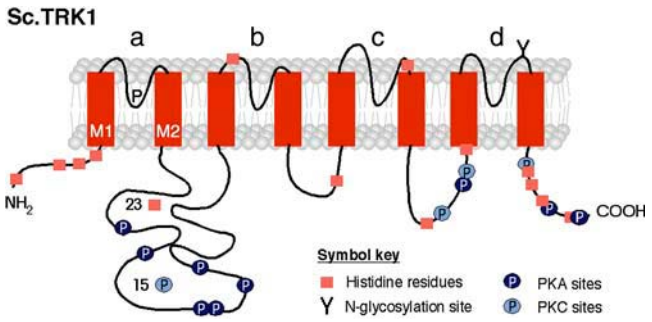

FIGURE 1 Bar-and-string diagram of the ScTRK1 protein, folded like a potassium channel. The primary folding subunit is a pair of transmembrane helices (*M1*, *M2*) sandwiching a recurrent loop (*P*), with strong sequence conservation among the four MPM units (*a–d*), and with significant similarity to bacterial potassium-channel sequences. Drawing is based on a detailed structure proposed by Durell and Guy (16) and supported by sidedness determinations on the ScTRK2 protein (see Ref. 21) and on several plant homologs.

below, chloride permeability, as distinct from conductance, is a stable property of the TRK proteins, independent of the actual cytoplasmic concentration of that ion. Finally, the kinetic form of the chloride currents, dependent upon the membrane voltage, is the same for both yeast TRK proteins, Trk1p and Trk2p, and is independent of their effective expression/activation levels, as determined by the *Saccharomyces*-strain background (22). The form is also quite different from that expected for diffusion through an ion-leakage pathway.

Two distinct models have been derived which are computationally equivalent for most of the accessible data: the first based on Nernst-Planck diffusion through a simple voltage-gated channel; the second based on voltage-driven flow through two chemical activation steps, in series within the membrane. Both models fit the data economically, requiring only a single intrinsic parameter to change systematically over each set of conditions, in the normal range of clamped membrane voltages, i.e., 20 mV to −200 mV for yeast spheroplasts. Sparing data at larger voltages, −200 to −300 mV, favor the second model.

MATERIALS AND METHODS

The background strains for all experiments in Figs. 2–4 were BS202 (*Mat***a**) and BS203 (*Matα*), with the genotype *ade2-1 can1-100 his3-11,15 leu2-3,112 trp1-1 ura3-1 lys2-ΔNhel* in the W303 background, as provided by Dr. Albert Smith (Yale Department of Molecular, Cellular, and Developmental Biology, New Haven, CT). Strains actually used for the experiments were EBC202/203, derived from BS202/203 by deletion of *PMR1* (*pmr1Δ::TRP1*), which encodes a Golgi-resident calcium pump; deletion of that gene/protein results in substantial enlargement of both intact cells and spheroplasts of *Saccharomyces*.

Quantitative I-V analysis of strain-background effects on the TRK-dependent chloride currents (Fig. 11) was made possible with strains provided by Dr. Per Ljungdahl (Ludwig Institute, Stockholm, Sweden) and derived from PLY232/248, which have the genotype *Mat***a**/*α his3-Δ200 leu2-3,112 trp1-Δ901 ura3-52 suc2-Δ9*, in the S288c background. Comparison of chloride currents with Trk1p and Trk2p expressed separately required several additional strains (detailed in Fig. 11 and its legend) constructed by deleting either *TRK1* or *TRK2* from BS202/203, EBC202/203, and PLY232/248, as already described (22).

Cells were normally grown in shaking liquid YPD medium (0.5% yeast extract, 0.5% bactopeptone, 2% glucose), at 30°C, to a final OD_{600} of 0.8–1.2. For strains carrying the *pmr1Δ* mutation, 10 mM $CaCl_2$ was added to the growth medium; and for *trk1Δ* strains, 90 mM KCl was added. Alternative ions (Cl^-, gluconate) were tested in the standard intracellular or extracellular buffers (see below) by direct substitution for molar-equivalent chloride. Glycerol, used in a few experiments at concentrations up to 10% w/v (~1 M; as osmotic stabilizer), had no readily observable deleterious effect on yeast, other than slight retardation of growth (doubling times of 1.9–2.1 h instead of the normal 1.75 h, at 30°C), as had already been demonstrated during its use as a chemical chaperone (21,28).

Cells were spheroplasted as previously described (29). Briefly, after harvesting from late exponential phase cultures, cells were washed in 50 mM KH_2PO_4 at pH 7.2, preincubated 0.5 h in the same buffer supplemented with 0.2% β-mercaptoethanol (β-ME; Buffer A), centrifuged, then resuspended in Buffer A plus 2.4 M sorbitol (Buffer B) containing 0.6 units of zymolyase 20T (Cat. 3320921, ICN Biomedicals, Irvine, CA), and incubated for 45 min at 30°C with slow nutation. The resulting spheroplasts were spun down, then gently resuspended in stabilizing buffer (Buffer C: 220 mM KCl, 10 mM $CaCl_2$, 5 mM $MgCl_2$, 5 mM MES brought to pH 7.2 with Tris base, + 0.2% glucose), where they could be maintained for several hours at 23°C, if necessary, before use. For recording, ~2 μl of suspension was pipetted directly onto the chamber bottom, and cells were allowed to settle (~10 min) and attach lightly to the chamber, before the chamber was flushed with the recording solution.

Recording solutions were simple modifications of those already described for patch-clamp studies of *Saccharomyces* (22,29). Buffer D (sealing buffer, extracellular) and Buffer 5.5 contained 150 mM KCl, 10 mM $CaCl_2$, 5 mM $MgCl_2$, 1 mM MES titrated to pH 7.5 (Buffer D), or to pH 5.5, with Tris base; and Buffer G (whole-cell pipette buffer), contained 175 mM KCl, 1 mM EGTA, 0.15 mM $CaCl_2$ (free Ca^{2+} = 100 nM), 4 mM $MgCl_2$, and 4 mM ATP, titrated to pH 7.0 with KOH. Chloride-depleted buffers were mostly prepared by equimolar K-gluconate replacement of the KCl present in Buffers D, 5.5, or G. Elevated intracellular chloride (258 and 591 mM, in Fig. 2), required 75 mM KCl or 408 mM KCl to be added, respectively, to Buffer G. Also, osmotic balance for the 591 mM chloride required addition of 1 M glycerol to all extracellular solutions, including growth medium (YPD), the spheroplasting solution, and Buffers C, D, and 5.5.

For the experiments in Fig. 10, testing the effects of (low) extracellular chloride on the TRK-dependent currents, Buffers G and 5.5 were replaced with zero-K^+, low Cl^- variants, i.e., pipette (intracellular) solution: 1 mM choline-Cl, 313 mM sorbitol, 1 mM EGTA, 0.15 mM Ca-gluconate, 4 mM Mg-gluconate, 4 mM Mg-ATP (pH 7.0); and bath solution: 1-3 mM choline-Cl, 265 mM sorbitol, 10 mM Ca-gluconate, 5 mM Mg-gluconate, 1 mM Mes-Tris pH 5.5. The 100-mM-chloride solution used in trials of Fig. 10 *B* (*upper curve*) was similar to the low-chloride version of Buffer 5.5, but contained only 90 mM sorbitol, with 100 mM choline chloride added.

Patch recording was accomplished with borosilicate pipettes connected to an EPC9 amplifier (22,29), which was managed by PULSE software (HEKA Elektronik, Lambrecht, Germany) via a PowerMacG4 computer (Apple Computer, Cupertino, CA). Yeast membrane currents were measured by whole-cell patch recording, using a staircase of 1.5-s or 2.5-s voltage pulses (from a holding voltage of −40 mV), to +100 mV, +80, . . .−180, −200 mV, in 20-mV decrements. Steady-state current-voltage curves (I-V curves) were generated by averaging the values sampled between 0.5 and 0.9 of the pulse width, and plotting the averages against clamped voltage for each pulse. The results were corrected for obvious current leakage by subtracting the Ohmic line corresponding to the minimal slope of the raw I-V curve near the origin (22). In these experiments, data were always collected between +100 mV and −180 or −200 mV, but the actual data displays (current records as well as I-V plots) were truncated at +20 mV, since positive (outward) currents were unrelated to the TRK proteins (22,30). Data were routinely collected at 2 kHz and filtered at 250 Hz.

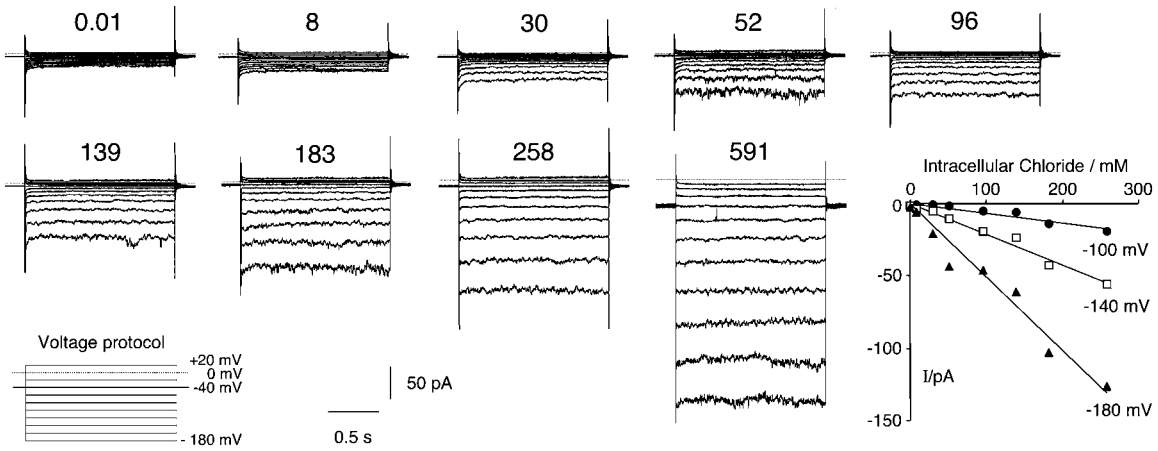

FIGURE 2 The amplitude of TRK-dependent current is proportional to the intracellular Cl^- concentration ($[Cl^-]_i$). (*Top nine panels*) Whole-cell recordings from nine different spheroplasts with patch pipettes containing Cl^- at concentrations indicated above each panel. (*Lower left panel*) Voltage-clamp protocol (superimposed tracings) used to generate currents in the upper panels: 1.5-s square pulses from a holding voltage of −40 mV to +20, 0, −20 . . . −180 in 20-mV decrements. (*Lower right panel*) Plot of the measured steady-state currents (I_m) at three values of membrane voltage (V_m): −100 mV, −140 mV, and −180 mV, to demonstrate the dependence on $[Cl^-]_i$. Symbols represent average currents calculated along each tracing in the interval 0.8–1.4 s, and straight lines are least-squares fits of the points, with intercepts forced to zero, and slopes found to be −0.067, −0.211, and −0.506 pA/mM, read from top downward. Each record set is representative of recordings from three or more spheroplasts. Yeast strain EBC202; extracellular pH (pH_o) was 5.5 in all experiments; $[Cl^-]_o$ = 195 mM; pH_i = 7.0. Cells and solutions prepared as described in Materials and Methods.

RESULTS

Detailed dependence of the major TRK-mediated currents upon cytosolic chloride

As a simple way to minimize both recording impedances and liquid-junction potentials, chloride-containing bridge solutions (KCl solutions) have customarily been used to fill microelectrodes for whole-cell patch recording. However, it was shown ~20 years ago that such solutions rapidly depolarize yeast-like cells of the mycelial fungus *Neurospora crassa* (31); and the likely cause of that depolarization can now be inferred to have been massive chloride efflux

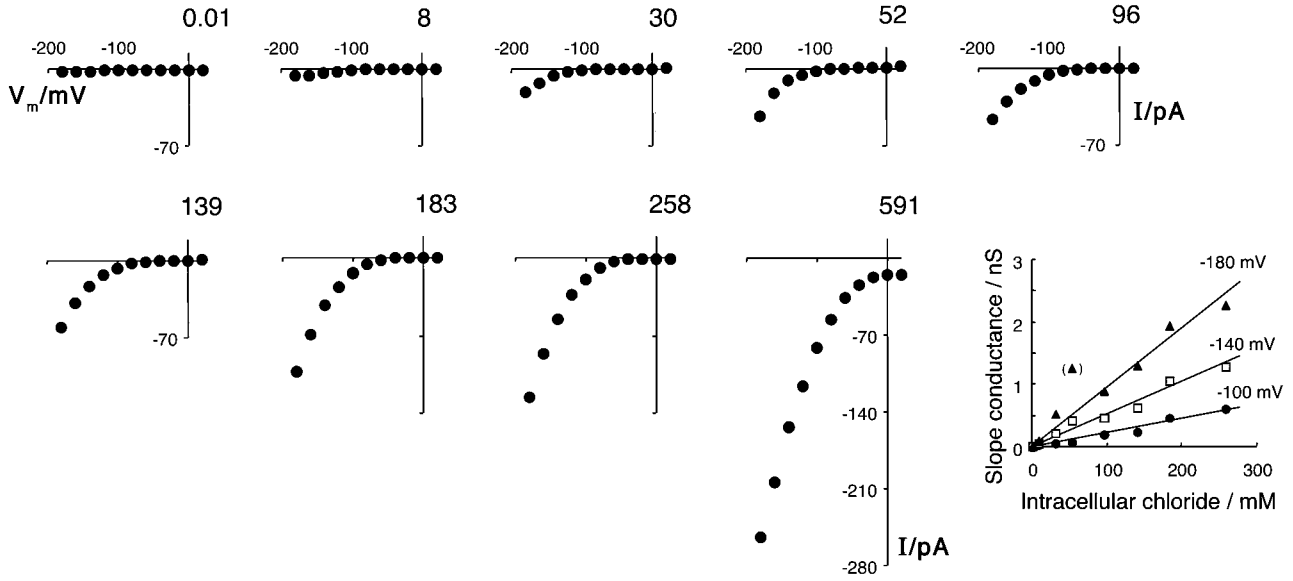

FIGURE 3 Steady-state current-voltage (I-V) plots corresponding to Fig. 2, emphasizing the strong inward rectification due to chloride efflux through the TRK proteins. (*Top nine panels*) Averaged currents for all records from comparable experiments (minimum of three spheroplasts for each value of $[Cl^-]_i$). All plots corrected for small Ohmic leakage currents (22). General description and conditions as for Fig. 2; axis scales at the top and right-hand side apply to all plots. (*Lower right panel*) Slope conductances at three voltages calculated from smoothing polynomials (fourth degree) fitted to the data plots. Conductance lines were fitted by least-squares, forced through the origin; slopes: 9.56, 5.29, and 2.35 pS/mM, read from top downward. Point in brackets (slope at −180 mV for $[Cl^-]_i$ = 52 mM) was omitted from the fit.

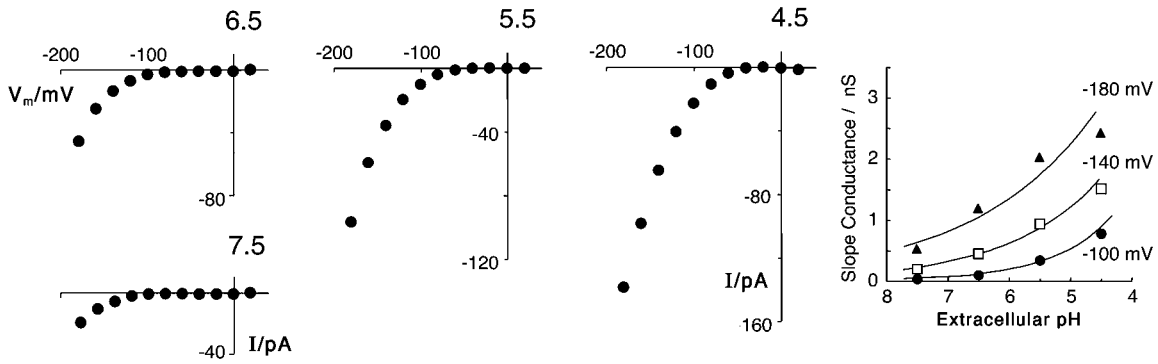

FIGURE 4 Steady-state I-V plots to demonstrate the strong dependence of chloride currents upon acidic extracellular pH. Protocols and general information as for Fig. 3. (*Right panel*) The logarithm of slope conductance was found to vary with pH (logarithm of H^+ concentration), but yielded Hill coefficients significantly less than unity: 0.22 (▲), 0.30 (□), and 0.46 (●), identifying H^+ ions as a modifier in the chloride transport process, rather than as a substrate. Plotted values of current, throughout, are averages from at least four spheroplasts, each having been measured at all four pH_o values.

through the *Neurospora* TRK protein. [In the eight transmembrane segments and four *P*-loops, NcTrk1p is 58% sequence-identical with Trk2p in *Saccharomyces*, and 75% homologous when conservative substitutions are included.] In patch-clamp experiments with yeast, reduction of pipette $[Cl^-]$ from 183 mM to 8 mM, by replacement of the usual 175 mM KCl with equivalent K-gluconate, reduced the TRK-dependent inward currents (anion efflux) by >90% (22). A more detailed demonstration of such results is shown in Fig. 2, for total intracellular chloride concentrations between 0 (assumed to be ~10 μM) and 591 mM, at an extracellular pH of 5.5. Required clamp currents were negative (*inward*; *downward* from the *dotted lines*) for almost all voltage pulses negative to 0 mV, and settled to their steady-state values within 50–75 ms. Furthermore, as is shown in the inset (*lower right panel*), these steady-state currents were proportional to the test chloride concentrations. Summary current-voltage plots of the steady-state currents (leak-corrected) are given in Fig. 3, which especially emphasizes the strong inwardly rectified characteristic of these TRK-mediated currents: e.g., slope conductances at −180 mV were typically fourfold larger than those at −100 mV, as is demonstrated especially by inset of Fig. 3 (*lower right panel*).

Both inset plots, for Figs. 2 and 3, have omitted the corresponding points for the highest chloride concentration tested, 591 mM, which in all cases were significantly smaller (lying closer to the abscissa) than predicted from regression lines drawn through all points for the lower concentrations. In other words, the I-V curve for $[Cl^-]_{in}$ = 591 mM was obviously distinct in shape, not just in scaling, from those for the other eight concentrations tested. Although a plausible simple interpretation of this fact has emerged from kinetic modeling (see below), the result may also have been influenced by the practical necessity for osmotic protection of cells to be tested with nearly ~600 mM intracellular (pipette) salt. Suitable protection was provided by supplementing buffers used for growth, spheroplasting, and stabilization with 1.2 M glycerol. At that concentration glycerol serves well in yeast both as the preferred compatible osmolyte (32) and as a chemical chaperone (21,28).

pH-Dependence of the TRK currents

Before the role of chloride was appreciated, Bihler et al. (30) noted a strong dependence of these large TRK-mediated currents on extracellular pH, with currents at any one clamped membrane voltage increasing in amplitude by six- to eightfold from pH_o 7.5 to 4.5. This occurred in such fashion that the I-V curve at pH_o 7.5, for instance, appeared simply to be displaced negatively along the voltage axis, ~110 mV negative compared with the I-V curve at pH_o 4.5. More detailed ensembles of records, similar to those of Fig. 2, have now been obtained, and the resultant average leak-corrected current-voltage curves are plotted in Fig. 4.

Superficially, these curves resemble the ones shown in Fig. 3 for variation of $[Cl^-]_i$, but there is no simple proportionality between the extracellular proton concentration and either the amplitude of current at any one voltage or the slope conductance of the I-V curves (Fig. 4, *inset*). The fact of this distinctly <10-fold increase of current, accompanying a 1000-fold increase of proton concentration, suggests *modulation* of the currents by pH_o, rather than a substrate-like interaction of protons with the transporters, such as that developed above for chloride ions. That protons cannot actually conduct the currents of Figs. 2–4 was previously inferred from the complete insensitivity of such currents to extracellular (H^+) buffer capacity (22).

The subtle difference in kinetic effect of changing pH_o, compared with changing $[Cl^-]_i$, is demonstrated by the

obviously nonlinear relationship of slope conductance to pH_o, which yields log-log slopes (Hill plots) much less than unity, viz. between 0.22 and 0.46 for the three voltages plotted. A quantitative understanding of these two sets of current-voltage relationships, with their well-defined dependence on cytosolic chloride concentration and on extracellular pH, can be obtained only by explicit kinetic modeling.

Two kinetic models for steady-state chloride currents mediated by the TRK proteins

Equations which reasonably describe the I-V relationships in Figs. 3 and 4 can be derived from two distinct classes of kinetic models.

The first—and most familiar—of these arises from the idea of Nernst-Planck diffusion of ions through a voltage-gated channel. Its simplest form applicable to observations of steady-state chloride current through the TRK proteins is

$$I_m = \phi\left[\frac{z_c^2F^2V_m}{RT}\right] \times\left[\frac{(P_{Cl}Cl_i + P_KK_o)\exp(z_cFV_m/RT) - (P_{Cl}Cl_o + P_KK_i)}{\exp(z_cFV_m/RT) - 1}\right] \times\left[\frac{\exp(z_gF(E_g - V_m)/RT)}{\exp(z_gF(E_g - V_m)/RT) + 1}\right], \quad (1)$$

in which I_m is the measured current, ϕ is an experimental scaling factor, and z_cF in the first bracketed term converts chemical flux to current; z_c, the valence of the diffusible ions, is taken as -1, since the major permeant ion is chloride. z_cFV_m/RT, in the first term, is the reduced membrane voltage, which combines with the second bracketed expression to describe constant-field diffusion of chloride and potassium (33); K_i, Cl_i and K_o, Cl_o are the intracellular and extracellular concentrations, respectively, of potassium and chloride ions, and P_K, P_{Cl} are the corresponding permeabilities.

The third bracketed expression represents the steady-state open probability (P_o) of a channel that is driven open by negative membrane voltages (V_m), driven closed by positive membrane voltages, and is poised half open at E_g, its characteristic gating voltage. Channel opening and closing are mediated via displacement of a gating charge, z_g, through the membrane dielectric. R, T, and F have their usual meanings. Equation 1 will be referred to as the *Gated-channel Model*.

A more general class of models, which would not require switch-like gating behavior of the TRK system, derives from the idea that membrane-transport processes—like conventional chemical reactions—occur via activated states, otherwise termed *energy barriers*. The simplest variant of this idea which can approximate the current-voltage data in Figs. 3 and 4 contains two barriers, α and β, located in series within the membrane dielectric, as depicted in Fig. 5 (*top panel*). Because this kind of model is much less familiar than the voltage-gated channel leading to Eq. 1, its mathematical formulation is presented in Appendix A. The resulting equation for steady-state membrane current is

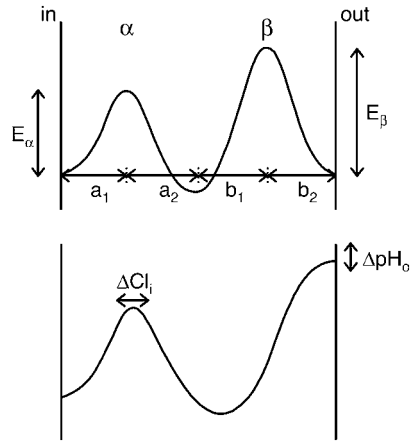

FIGURE 5 Activation-energy diagram for a two-barrier mechanism of chloride transport. (*Top panel*) Definition of terms. Barriers α and β represent activation energies E_α and E_β, and are positioned at distances a_1 and b_2, respectively, from the surfaces of the membrane dielectric. (*Bottom panel*) Diagram adjusted roughly for the relative heights and positions of the barriers, deduced from data analysis, as influenced by changing chloride concentration (ΔCl_i) and changing pH (ΔpH_o).

$$I_m = \phi z_cF\frac{Cl_i\exp(z_cFa_1V_m/RT) - Cl_o\exp(-z_cF(1-a_1)V_m/RT)}{A + B\exp(-z_cF(1-a_1-b_2)V_m/RT)}, \quad (2)$$

where symbols common to Eq. 1 have the same meanings. a_1 represents the fractional distance of barrier α from the inner face of the membrane dielectric, b_2 represents the fractional distance of barrier β from the outer face of the membrane dielectric, $A = \exp(E_\alpha/RT)$ is the reciprocal of the Boltzmann expression relating reaction velocity to activation energy (E_α) at barrier α, and $B = \exp(E_\beta/RT)$ is the corresponding term for barrier β. Equation 2 will be referred to as the *Two-barrier Model*.

Both models contain four intrinsic parameters which could control the detailed shapes of calculated current-voltage curves under different experimental conditions. In the gated-channel model (Eq. 1), those are P_{Cl}, P_K, z_g, and E_g; in the two-barrier model, they are a_1, b_2, A, and B. However, in practice both models displayed only three variable intrinsic parameters, because P_K could be fixed at a small value and was completely unnecessary except at the lowest two chloride concentrations (~0.01 mM, 8.3 mM); and because b_2 always assumed its minimal value (zero) in parameter optimization runs. The resultant implied shape of the double

barrier is depicted diagrammatically in Fig. 5 (*bottom panel*). Finally, the extrinsic parameter ϕ, a pure scaling factor, was again required to deal with the scattered sizes of yeast protoplasts that are patchable under the normal conditions of these experiments.

Both models fit the pH-dependence data, and with only one pH-dependent parameter

The clearest results obtained when all variations of the test conditions could be executed on every spheroplast studied. Such was possible, and routine, when extracellular pH was varied, i.e., to generate the plots of Fig. 4. Then ϕ could be fixed at unity, and the fitting algorithm (34) was arranged so that two of the three parameters in each model were obtained in common for all four current-voltage curves, whereas the third was allowed to vary from one curve to the next. The resulting optimal fits of the two models are shown separately in Fig. 6, and examination of the two panels shows clear differences, but they are small. Both curves fitting each I-V plot were qualitatively satisfactory; and statistically, neither model differed significantly from the data, except for the small-current points at pH 4.5 (V_m positive to −80 mV), as indicated by the X^2 values in Table 1. Also, there were no significant differences between the two models. The optimized parameter values are given in Table 1. In the gated-channel model, only E_g, the apparent gating voltage, varied from one pH to the next; and in the two-barrier model, only parameter B, reflecting the height of the outer barrier, varied from curve to curve. Thus, either the apparent gating voltage-shifted positive as pH_o fell (Eq. 1), or the height of the outer barrier diminished (Eq. 2). Both dependencies were linear with pH, as demonstrated by the plots of Fig. 7. The calculated E_g shifted positive 37.1 mV for each unit decline of pH_o, from −266 mV at pH 7.5; and the calculated activation energy, E_β, diminished by 0.69 Kcal/mole for each unit decline of pH_o, from a value of 12.5 Kcal/mole at pH 7.5. That slope for E_β would correspond to a voltage slope of 30.1 mV/pH unit, ~20% less than the voltage slope found in the gated-channel model.

TABLE 1 Fitting parameters for pH_o effects on the TRK-mediated chloride currents (Fig. 6)

Gated-channel model				
pH_o	7.5	6.5	5.5	4.5
ϕ	≡ 1.0	≡ 1.0	≡ 1.0	≡ 1.0
P_{Cl} (10^{-6} cm/s)	0.861	0.861	0.861	0.861
E_g (mV)	−267	−231	−188	−157
z_g	≡ 0.674	≡ 0.674	≡ 0.674	≡ 0.674
X^2 (from fit)	4.3	2.2	7.8	18.8*
Two-barrier model				
pH_o	7.5	6.5	5.5	4.5
ϕ (cm/s)	≡ 1.0	≡ 1.0	≡ 1.0	≡ 1.0
a_1	0.253	0.253	0.253	0.253
b_2	≡ 0.0	≡ 0.0	≡ 0.0	≡ 0.0
A	1.22×10^6	1.22×10^6	1.22×10^6	1.22×10^6
B	1.72×10^9	6.28×10^8	1.70×10^8	5.40×10^7
E_α (Kcal/mole)	8.24	8.24	8.24	8.24
E_β (Kcal/mole)	12.5	11.9	11.1	10.5
X^2 (from fit)	2.3	1.9	5.8	23.4†
X^2 (btwn models)	1.3	1.7	1.3	0.4

All data in Fig. 4, replotted in Fig. 6, were fitted collectively to text Eq. 1, for the upper panel; and to text Eq. 2, for the lower panel. The identity symbol (≡) means that each value was preassigned. For z_g, the assigned value was taken from the separate analysis of chloride effects (see Fig. 7 and Table 2). ϕ was set equal to unity for these pH experiments, since each protoplast was tested at all four values of pH_o. See legend to Fig. 6 for additional details. The reported values of A and B are proportional to the average surface areas of the cells studied, and the values of P_{Cl} and P_K are inversely related to cell surface area. 200 μm^2 was assumed, since 8.0 μm = the rough average diameter for *pmr1*Δ spheroplasts used in the patch-clamp experiments of Fig. 4.

*Significant difference: ρ ~0.03 (9 degrees of freedom).

†Significant difference: ρ ~0.005 (8 df).

Both models fit the chloride-dependence data, also with only one Cl^--dependent parameter

Optimal fits of both models, to all nine I-V plots from Fig. 3, are displayed in Fig. 8, with the solid curves representing the two-barrier model, and the dashed curves representing the gated-channel model. The corresponding parameter values are listed in Table 2. Again, the fitted curves did not differ significantly from the data. However, the fact that a new spheroplast was used for each change of $[Cl^-]_i$ introduced

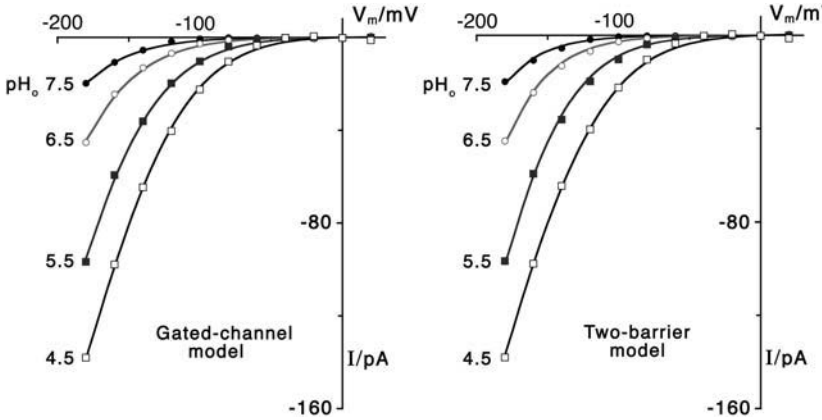

FIGURE 6 Goodness-of-fit demonstrations for the two models and the I-V plots of Fig. 4, at all four values of extracellular pH. The Marquardt algorithm (34) for nonlinear least-squares was used to calculate the fits jointly for all four data sets, holding three parameters in common, within each model. Parameter values are listed in Table 1. (*Left panel*) Gated-channel model, see Eq. 1. The values P_K and ϕ were fixed. Only E_g was required to vary with pH. (*Right panel*) Two-barrier model, text Eq. 2. The values b_2 and ϕ were fixed. Only B (E_β) was required to vary with pH. There are no statistically significant deviations between the fitted curves and the plots, except for the low-voltage points (positive to −80 mV) at pH_o 4.5 (see Table 1).

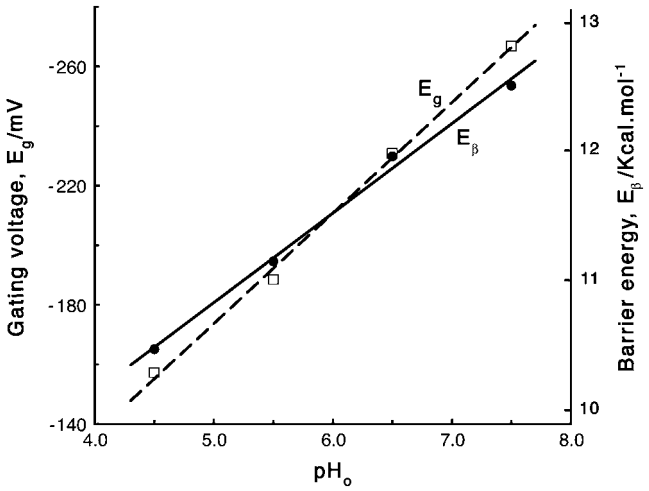

FIGURE 7 Linear variation of the pH-dependent parameters, E_g and E_β, from Fig. 6. E_β (●, *right ordinate scale*) was calculated from the fitted values of B: $E_\beta = RT \ln(B)$, and the plot was scaled to make the slope of the regression line, 0.69 Kcal mol^{-1}/pH unit, correspond to voltage, i.e., 30.1 mV/pH unit. Values of E_g (□) were taken directly from the fitted results, and have a regression slope of 37.1 mV/pH unit.

substantial randomness of cell size (surface area) into the measurements, which is reflected by scattered values of the scaling factor ϕ. That parameter was fixed at unity for the standard condition ($pH_o = 5.5$, $[Cl^-]_i = 183.3$ mM), and it changed generally in the same direction, for the two models, at each other chloride concentration; but the optimized values were certainly not identical between the two models.

Among the model-intrinsic parameters, only one in each model needed to change with chloride concentration: z_g in Eq. 1, and a_1 in Eq. 2. That is, raising intracellular chloride reduced the apparent gating charge for channel opening, from ~1.0 at low $[Cl^-]_i$ to ~0.5 at high chloride; or, it reduced the distance separating the activation barrier α from the inner surface of the membrane dielectric, from ~0.4 at low chloride to ~0.2 at high $[Cl^-]_i$. These parameters, both of which affect the spread of the exponential expressions, in Eq. 1 or Eq. 2, impinge on the shape of the I-V curves, not just upon their scale. As is demonstrated in Fig. 9, both parameters, z_g and a_1, appeared to vary as simple exponential functions of $[Cl^-]_i$. The computed rate constants for this decline differed by ~20%, again, as had the slopes of parameters E_g and E_β, varying with extracellular pH. Anomalously low values were also found for z_g and a_1 at the lowest cytoplasmic chloride concentration, implying a discontinuity in the behavior of the measured currents with very low chloride.

Influence of the extracellular chloride concentration

Two special points must be made about these chloride-dependent currents through the TRK proteins, but it is sufficient to make them via a single model, without the detailed comparisons of Eq. 1 with Eq. 2. The first point is that when the intracellular chloride concentration was low, extracellular chloride clearly modulated chloride permeability.

These experiments were initially conducted as a boundary test of Eq. 1: potassium was omitted from both intracellular and extracellular solutions, and extracellular chloride concentration, $[Cl^-]_o$, was varied to examine the experimental reversal voltage for chloride currents through the TRK proteins, without the complication of simultaneously altering their steady-state amplitudes. That experiment failed as such, because of small (~0.3 pA) random offset currents that could not be corralled. However, when a fixed current was subtracted from each experimental I-V plot, sufficient

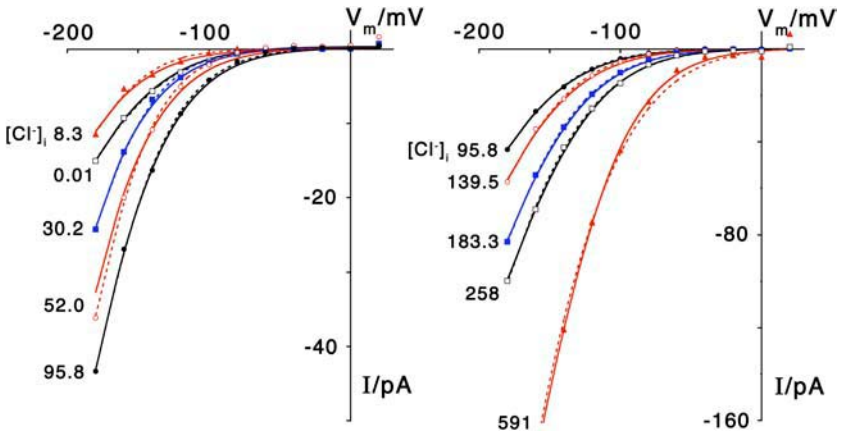

FIGURE 8 Goodness-of-fit demonstrations for the two models and the I-V plots of Fig. 3, at all nine concentrations of intracellular chloride. General mechanics and strategy of fitting were similar to those of Fig. 6. Parameter values are listed in Table 2. (*Left panel*) $[Cl^-]_i$ from 0.01 mM to 95.8 mM. (*Right panel*) $[Cl^-]_i$ from 95.8 mM to 591 mM. Plot and curves for 95.8 mM are shown in both panels, to emphasize the change in ordinate scale between the two panels. (*Dashed curves*) Gated-channel model, see Eq. 1. P_K was fixed; only z_g varied systematically with $[Cl^-]_i$. (*Solid curves*) Two-barrier model, see Eq. 2. b_2 was fixed. Only a_1 varied systematically with $[Cl^-]_i$. ϕ was found separately for each plot (see Table 2; set equal to unity for 183.3 mM chloride), to accommodate differences in physical size of spheroplasts selected for patch-recording. There are no statistically significant deviations between the fitted curves and the plots, except for the low-voltage points (positive to −80 mV) at 591 mM chloride. [Note that at very low $[Cl^-]_i$, 0.01 mM and 8.3 mM in these experiments, Eqs. 1 and 2 both require accounting for residual permeability to other ions, assumed in Eq. 1 to be potassium: thus, P_K. Because there is no accepted simple convention to include other ions in formulation of Eq. 2, a pseudo-concentration term, = 19.3 mM, was added to the actual 0.01 mM and 8.3 mM to make those two I-V curves compatible with the other seven].

TABLE 2 Fitting parameters for $[Cl^-]_i$ effects on the TRK-mediated chloride currents (Fig. 8)

Gated-channel model									
$[Cl^-]_i$ (mM)	0.01	8.3	30.2	52.0	95.8	139.5	183.3	258	591
ϕ	1.15	0.687	0.974	1.08	0.863	0.848	$\equiv$ 1.0	0.848	0.848
P_{Cl} (10^{-6} cm/s)	0.635	0.635	0.635	0.635	0.635	0.635	0.635	0.635	0.635
P_K (10^{-6} cm/s)	$\equiv$ 0.14	$\equiv$ 0.14	$\equiv$ 0.14	$\equiv$ 0.14	$\equiv$ 0.14	$\equiv$ 0.14	$\equiv$ 0.14	$\equiv$ 0.14	$\equiv$ 0.14
E_g (mV)	−179	−179	−179	−179	−179	−179	−179	−179	−179
z_g	0.715	1.02	0.919	0.942	0.754	0.761	0.674	0.620	0.521
X^2 (from fit)	0.41	1.97	1.30	4.29	2.08	1.26	1.83	2.24	14.6*
Two-barrier model									
$[Cl^-]_i$ (mM)	0.01	8.3	30.2	52.0	95.8	139.5	183.3	258	591
ϕ (cm/s)	1.42	0.517	1.051	0.906	0.807	0.764	$\equiv$ 1.0	0.983	1.33
a_1	0.320	0.399	0.393	0.371	0.323	0.312	0.279	0.254	0.209
b_2	$\equiv$ 0.0	$\equiv$ 0.0	$\equiv$ 0.0	$\equiv$ 0.0	$\equiv$ 0.0	$\equiv$ 0.0	$\equiv$ 0.0	$\equiv$ 0.0	$\equiv$ 0.0
A	2.24×10^6	2.24×10^6	2.24×10^6	2.24×10^6	2.24×10^6	2.24×10^6	2.24×10^6	2.24×10^6	2.24×10^6
B	1.24×10^9	1.24×10^9	1.24×10^9	1.24×10^9	1.24×10^9	1.24×10^9	1.24×10^9	1.24×10^9	1.24×10^9
E_α (Kcal/mole)	8.60	8.60	8.60	8.60	8.60	8.60	8.60	8.60	8.60
E_β (Kcal/mole)	10.97	10.97	10.97	10.97	10.97	10.97	10.97	10.97	10.97
X^2 (from fit)	0.44	3.34	3.13	6.60	2.84	2.64	2.61	2.13	10.12
X^2 (between models)	0.65	0.97	1.64	1.76	0.28	0.87	0.21	0.11	2.7

All data in Figs. 3 and 8 were fitted collectively to text Eq. 1, for the upper panel; and to text Eq. 2, for the lower panel. Symbol notes as for Table 1. Fits were optimized with parameters found as indicated: In the gated-channel model (Eq. 1), gating voltage (E_g) and chloride permeability (P_{Cl}) were found in common for all nine plots, whereas the apparent gating charge (z_g) and size-scaling factor (ϕ) were found for each curve. The assumed standard cell size was 8-μm diameter, 200-μm^2 surface area. In the two-barrier model (Eq. 2), A and B were found in common for all nine plots, and ϕ and a_1 (the position of barrier α) were found separately. The resulting curves did not differ significantly from the data plots, except for Eq. 2 at the highest chloride concentration.

*Significant difference: $\rho \sim 0.07$ (7 df).

to *force* the plot through the calculated chloride-reversal voltage (E_{Cl}), the effect of $[Cl^-]_o$ on total current became apparent. Summary data, with fits to the gated-channel model, are shown separately in Fig. 10 for high (183.3 mM) and low (1–3 mM) $[Cl^-]_i$. The data in Fig. 10 *A*, with $[Cl^-]_i$ = 183 mM, yielded $P_{Cl} = 0.97 \times 10^{-6}$ cm/s at high extracellular chloride, and a hardly significant increase—to 1.15×10^{-6} cm/ s—at very low $[Cl^-]_o$. These numbers were comfortably close to the range obtained from the fits of Figs. 6 and 8 (Tables 1 and 2), that is, 0.635–0.861 $\times 10^{-6}$ cm/s. The data in Fig. 10 *B*, for low intracellular chloride, yielded distinctly larger values of P_{Cl}: 1.54×10^{-6} cm/s at $[Cl^-]_o$ = 100 mM, and 2.90×10^{-6} cm/s for $[Cl^-]_o$ in the range 1–3 mM. These values proved significantly different with $\rho < 0.005$ (Student's *t*-test), demonstrating that the chloride permeability of the TRK proteins could be modulated by extracellular $[Cl^-]$, but that such modulation was evident only when intracellular $[Cl^-]$ was low. [Note that since low Cl^- and K^+ concentrations, both intracellular and extracellular, were achieved in these experiments partly by replacing KCl with sorbitol, it is possible that ionic strength—not purely chloride concentration—affected P_{Cl}.] However, whether the observed changes reflected altered selectivity in the ion-channeling process remains to be determined.

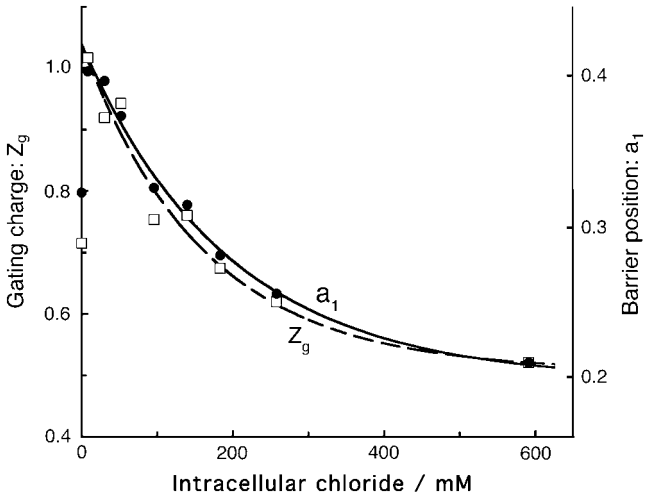

FIGURE 9 Exponential variation of the chloride-dependent parameters, z_g and a_1, from Fig. 8. Both sets of points represent the fitted values (see Table 2), and the plots are scaled so the extrapolated maximal values coincide at 0 $[Cl^-]_i$: 1.04 for z_g, and 0.42 for a_1. The exponential slope constants for the two parameters are 0.0062 and 0.0052; and the offsets (limiting values at very high chloride concentration) are 0.51 and 0.20, respectively. Points plotted near 0.7 and 0.8 on the left ordinate scale (for $[Cl^-]_i = 0.01$ mM) were excluded from the fits.

A further surprise in the results of Fig. 10 *B* was that Eq. 1 could not be fitted to the observed steady-state I-V curves when $z_g = 1$, predicted along the fitted curve of Fig. 9 (*solid circles*). A much lower value, near 0.7, was required, again consistent with the anomalous value actually plotted in Fig. 9 for $[Cl^-]_i$ near zero. This finding reinforces the notion of a functional discontinuity in chloride permeability at very low intracellular chloride concentrations.

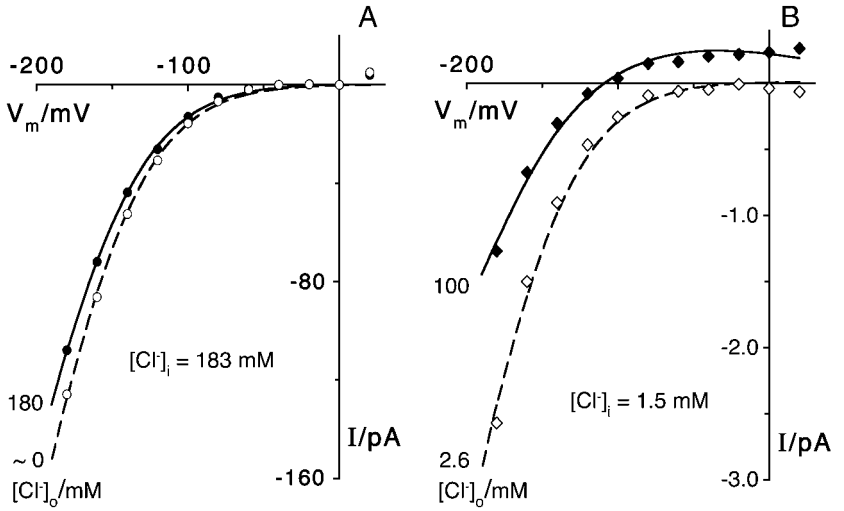

FIGURE 10 Given low $[Cl^-]_i$, extracellular chloride also modulates chloride efflux. (*A*) $[Cl^-]_i = 183.3$ mM, pipette solution was buffer G. For patch-recording, gigaseals were obtained in Buffer 5.5 ($pH_o = 5.5$, $[Cl^-]_o = 180$ mM) and, after the control voltage-clamp sequence was run at least once, $[Cl^-]_o$ was dropped by perfusing the chamber with chloride-free Buffer 5.5 (gluconate buffer; see Materials and Methods). (*B*) $[Cl^-]_i$ ~1.5 mM, pipette solution contained ~0 K^+ and 1.5 mM chloride. Gigaseals were obtained in modified Buffer 5.5, containing ~0 mM K^+ and 100 mM Cl^-; and again, after the control voltage-clamp sequence was run, buffer chloride was lowered, to 1–3 mM with different spheroplasts, averaging 2.6 mM. Each panel represents averages of paired measurements on 3–5 single spheroplasts, so the cell-size factor (ϕ) could be set to unity throughout. The smooth curves all represent Eq. 1 (gated-channel model) fitted to the data with $E_g = -178.8$ mV, $z_g = 0.674$ (both taken from Table 2), and $P_K = 0$. Only the apparent chloride permeability needed to be adjusted: P_{Cl} (10^{-6} cm/s) = 0.97, 1.15, 1.54, and 2.90, reading from top downward in *A*, then in *B*. Strain EBC 202 (TRK1 TRK2 TOK1 *pmr1*Δ) used throughout. Note the ~ 50-fold expansion of the ordinate scale from *A* to *B*, due to the much smaller chloride currents at low millimolar $[Cl^-]_i$.

The second special point: Trk1p and Trk2p are kinetically identical, with respect to chloride currents

Previous studies of the TRK proteins had observed significant dependences of current amplitude upon strain background (i.e., W303 versus S288c) and upon cell size (22,30,35). In fact, the proof that both proteins—Trk1p and Trk2p—contribute significantly to total chloride currents made use of background- and size-comparisons for three genotypes: wild-type (*TRK1 TRK2*), TRK2-deleted (*TRK1 trk2*Δ), and TRK1-deleted (*trk1*Δ *TRK2*). For each background/cell size, the amplitude of chloride current in the wild-type approximately equaled the sum of chloride currents in the TRK1-deleted and TRK2-deleted strains (22). Fitting of Eq. 1 to these data demonstrated that the gating parameters, E_g and z_g, were stable and independent of cell-size or expression level. Analysis of these experiments—which were completely independent of those in Figs. 3 and 8—is displayed in Fig. 11. All parameters could be fixed at the values from Figs. 8, except for P_{Cl} and—in the case of

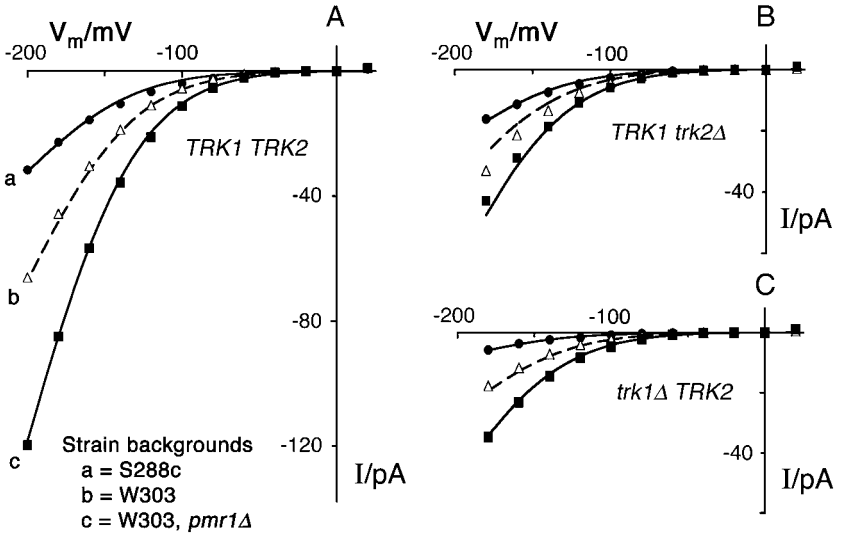

FIGURE 11 Trk1p and Trk2p are kinetically identical with respect to chloride currents, across strain backgrounds and cell sizes. All experiments were conducted at $pH_o = 5.5$ and $[Cl^-]_i = 183$ mM, and Eq. 1 was fitted with the same parameters determined for Fig. 8 (Table 2, gated-channel model), except for ϕ (cell size) and P_{Cl}. (*A*) Wild-type expression of Trk1p and Trk2p; strains PLY232, BS202, and EBC202 (*curves a*, *b*, and *c*, respectively). (*B*) Only Trk1p expressed; strains PLY236, EBF202, and EBJ 202 (read from *top downward*). (*C*) Only Trk2p expressed; strains PLY234, EBE203, and EBH203 (read from *top downward*). ϕ was set at unity for all the spheroplasts enlarged by *pmr1*Δ, i.e., the lower curve in each panel. All of the normal-sized spheroplasts were assumed to have a common value of ϕ, optimized at 0.567 by the fitting procedure. Values of P_{Cl} were found separately for each plot in the S288c background (*a*, *top* in each panel), and in common for each pair in the W303 background (*b*; c-*pmr1*Δ). Growth medium for *trk1*Δ strains was supplemented with 90 mM KCl, and all cells were maintained in elevated potassium (150–220 mM) after spheroplasting (see Materials and Methods). Plotted points taken from Fig. 7 of Kuroda et al. (22), but curves here are fitted (Eq. 1), not drawn point-to-point. Parameter values listed in Table 3.

small cells (wild-type for *PMR1*)—the scaling parameter ϕ. Fitted parameter values and other details are given in Table 3.

Although the fits with these constraints were not perfect, the deviations proved significant only for strains EBF202 (*trk2*Δ, Fig. 11 *B*) and EBE203 (*trk1*Δ, Fig. 11 *C*) in the W303 background; and the computed deviations clearly could have been eliminated by slightly different average cell sizes for those two strains, relative to the PLY strains (S288c background). The apparent chloride permeabilities have been taken to reflect expression densities of functional TRK protein in each strain, and agreement between the sums for the paired deletion strains and their corresponding wild-type strain complements the agreement of simple amplitudes previously demonstrated (22); i.e., in column 1 of Table 3, $0.266 + 0.092 = 0.358 \sim 0.366$; and in columns 2 and 3, $0.426 + 0.306 = 0.732 \sim 0.762$.

Rationalizing the models: What should happen at extreme voltages?

Within the realm of data suitable for quantitative analysis, there is no significant difference between the gated-channel model for chloride movement through the TRK proteins, and the two-barrier model. But clear distinctions should emerge, in principle, at large voltages, recalling that $z_c = -1$ in both Eqs. 1 and 2, and that $z_g > 0$, I_m (Eq. 1) $\rightarrow 0$ for large positive V_m, because the gating factor (third bracketed term) approaches zero. I_m (Eq. 2), on the other hand, resembles a *sinh* function, rising exponentially with large positive V_m. Unfortunately, the yeast plasma membrane breaks down rapidly at clamped voltages positive to +100 mV, even in strains with the conspicuous outwardly rectifying K^+ channel, Tok1p, deleted. Thus, it has not been possible to collect data over a range of positive membrane voltages suitable to distinguish between the two kinetic models.

Circumstances proved somewhat more favorable for large negative membrane voltages, where the yeast spheroplast membrane occasionally tolerated clamped voltages as large as −300 mV, thereby resembling the better-studied ascomycete *Neurospora*. In that realm, the gated channel model approaches a linear, Ohmic current-voltage relationship, while the two-barrier model, again, resembles a *sinh* function, falling exponentially with large negative V_m. Explicitly,

$$\lim_{V_m \rightarrow -\infty} I_m(\text{Eq. 1}) = \phi \left[\frac{z_c^2 F^2 V_m}{RT}\right][P_{Cl} Cl_i + P_K K_o], \qquad (3)$$

and

$$\lim_{V_m \rightarrow -\infty} I_m(\text{Eq. 2}) = \phi \left[\frac{z_c F Cl_i}{A}\right] \exp(z_c F a_1 V_m / RT), \qquad (4)$$

where not only the limiting exponential dependence of I_m on V_m is apparent, but also the fact that the parameter A in Eq. 2

TABLE 3 Parameter values for fitting Eq. 1 to multistrain data on TRK-dependent chloride currents (Fig. 11)

Genotype: *TRK1 TRK2*			
Strain	PLY232	BS202	EBC202
Background	S288c	W303	W303, *pmr1*Δ
ϕ (cm/s)	0.567	0.567	≡1.00
P_{Cl} (10^{-6} cm/s)	0.366	0.762	0.762
E_g (mV)	≡ −178.8	≡ −178.8	≡ −178.8
z_g	≡ 0.674	≡ 0.674	≡ 0.674
Genotype: *TRK1 trk2*Δ			
Strain	PLY236	EBF202	EBJ202
Background	S288c	W303	W303, *pmr1*Δ
ϕ (cm/s)	0.567	0.567	≡ 1.00
P_{Cl} (10^{-6} cm/s)	0.266	0.426	0.426
E_g (mV)	≡ −178.8	≡ −178.8	≡ −178.8
z_g	≡ 0.674	≡ 0.674	≡ 0.674
Genotype: *trk1*Δ *TRK2*			
Strain	PLY234	EBE203	EBH203
Background	S288c	W303	W303, *pmr1*Δ
ϕ (cm/s)	0.567	0.567	≡ 1.00
P_{Cl} (10^{-6} cm/s)	0.092	0.306	0.306
E_g (mV)	≡ −178.8	≡ −178.8	≡ −178.8
z_g	≡ 0.674	≡ 0.674	≡ 0.674

All data in Fig. 11 were fitted jointly to Eq. 1. The identity symbol (≡) denotes values preassigned from fits of Fig. 8, for E_g and z_g; and arbitrarily for $\phi \equiv 1$ (*right-hand column*), representing a standard surface area of ~200 μm^2, for *pmr1*Δ cells. The small cells (wild-type *PMR1*) were selected for nearly uniform size, and the resulting current data could be fitted with a common ϕ for all six cases. P_{Cl} was found in common for spheroplasts of the two W303 backgrounds within each TRK genotype. P_K was insignificant with $[Cl^-]_i$ >100 mM, and was set to zero for these fits.

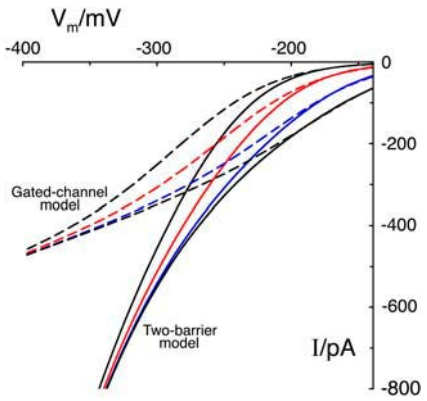

FIGURE 12 Theoretical discrimination between the two models at large negative membrane voltages. (*Upper set of curves*) Equation 1 using parameter values from Table 1 (*upper section*). (*Lower set of curves*) Equation 2 using parameter values from Table 2 (*lower section*). Values of pH_o, read from top down, are 7.5 (*black*), 6.5 (*red*), 5.5 (*blue*), and 4.5 (*black*). Limiting behavior for the gated-channel model is Eq. 3; limiting behavior for the two-barrier model is Eq. 4. Note that the paired curves are nearly identical for V_m positive to −200 mV, coinciding with the curves in Fig. 6. Scale on the abscissa begins at −140 mV.

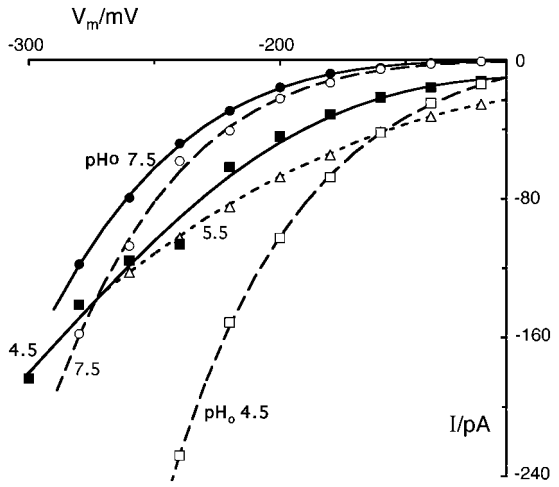

FIGURE 13 All available data show continuously increasing slope conductances at voltages beyond −200 mV. Only these five spheroplasts tolerated voltage-clamping at −220 to −300 mV. Standard recording conditions, as for Figs. 2–4; two cells at pH_o 7.5, two at pH_o 4.5, and one at pH_o 5.5. Scale on the abscissa begins at −110 mV.

functions as the reciprocal of permeability. The extended I-V curves for both models are drawn in Fig. 12, with parameter values from Table 1 for the four different values of pH_o. The single Ohmic asymptote for Eq. 1 (*upper four curves*) is evident, and the coincident and increasingly steep slopes of Eq. 2 are also clear.

These curves, taken pairwise, are essentially identical out to $V_m \approx -200$ mV, but deviate significantly by −225 mV and convincingly by −250 mV. Five yeast spheroplasts—out of the several hundred studied in these experiments—permitted a comparison, and are demonstrated in Fig. 13. Curves through these five I-V plots were drawn by eye, without prejudice of fitting to either model. None of them showed an inflection, which should have been evident by the gated-channel model—near −280 mV for data at pH 7.5, and near −220 mV for pH 4.5. In other words, all of these data plots extrapolate increasingly steeply toward more negative membrane voltages, a qualitative result which is consistent with the two-barrier model, but not with the gated-channel model.

DISCUSSION

Physiological significance

The observed large chloride currents are almost certainly an adventitious function of the yeast TRK proteins, rather than an evolved function. *Saccharomyces* requires no more than trace chloride for normal growth, and actual cytoplasmic concentrations much higher than 30 mM—i.e., sufficient to produce physiological currents like those demonstrated in most panels of Fig. 2—should short-circuit the proton pump and strongly inhibit the majority of voltage-dependent, proton-coupled nutrient transporters and drug efflux systems at the cell surface. Such deleterious effects of chloride leakage from microelectrodes have also been well demonstrated in other systems (31,36). Massive chloride efflux, if it is ever required physiologically by yeast, should be accomplished by electroneutral transport of salt or exchange of anions, and the demonstrated chloride permeability of TRK proteins probably plays only the limited role of providing a trickle pathway for voltage-driven exit of chloride.

Choice of kinetic models

The normal function of TRK proteins, in fungi, bacteria, and most plants, is well established to be net uptake of potassium sufficient to maintain intracellular K^+ concentration near ~200 mM, during rapid growth of the organism. Net transport via the TRK proteins, absent competing systems for K^+ influx or efflux, should therefore equal the product of steady-state internal concentration and growth rate, which is ~1 mM/min for *Saccharomyces*. That is ~10% of the maximal K^+ influx afforded by the TRK systems in yeast, and ~1% of the currents described above, under standard recording conditions ($pH_o = 5.5$, $[Cl^-]_i = 183$ mM, $V_m = -180$ mV). The measured chloride currents, then, are very large compared with normal carrier-mediated potassium currents through the TRK proteins, and elicit the notion of channel behavior, which has given rise to the explicit voltage-gated channel model of Eq. 1. That model makes a conceptual distinction between the mechanism of charge movement, per se, which would be diffusion along chloride's electrochemical gradient, and accessibility via a voltage-activated gate lying astride—rather than within—the transport pathway.

The alternative model, in Eq. 2, also requires two discrete processes, but they are conceptually and formally homologous and should both lie within the transport pathway, where the membrane's electric field would boost chloride ions through the controlling chemical or physical reactions. Although it has been realized for more than 30 years that activation-energy-barrier models of this sort could, in principle, describe the kinetic behavior of both conventional ion channels and carrier-type ion transporters (37–39), few attempts have been reported at quantitative comparison of the two classes of models on single homogeneous sets of data.

Our preference for the two-barrier model, rather than the voltage-gated channel model, rests first on the difficult-to-obtain data at very high (−) membrane voltages, where conductance was found to increase continuously with voltage (Fig. 13). Our preference rests second on the fact that specific kinetic effects of changing $[Cl^-]_i$ and pH_o separate cleanly into parameters naturally associated with the inner surface (a_1) and outer surface (E_β) of the cell membrane, consistent with the pre-existing structural model described below.

The central-pore hypothesis: Does Cl^- traverse the axial channel of TRK oligomers?

Durell and Guy (16), in drawing the first atomic-scale models of TRK-family proteins, not only predicted the K^+-channel-like folding of these molecules, which has since been confirmed (18,19,21), but also argued that proteins in the fungal subfamily could well oligomerize into dimers or tetramers. Motivation for this idea came from the observation that unexpectedly high degrees of sequence conservation and hydrophilicity persist in residues forming the transmembrane helices of fungal TRK proteins, particularly M2c, M1d, and M2d (see Fig. 1), so that a substantial fraction of conserved, hydrophilic residues should face the membrane's phospholipids, not just the interior of the postulated K^+ channel. Since little sequence conservation is expected among residues principally forming a hydrophobic interface within the membrane, Durell and Guy proposed a more specific function for the conserved residues, i.e., to cluster the monomers. In that way, conserved and hydrophilic residues on one molecule could complement those on another molecule, without exposure to the membrane lipids. The most compact variant of this idea was the tetramer shown in Fig. 5 of Ref. 16, for the SpTRK1 homolog from *Schizosaccharomyces pombe*.

Coordinates from that construct were used to generate Fig. 14, showing the entire tetramer in *A*, then ribbon (*B* and *D*) and space-filling diagrams (*C* and *E*) of the helices immediately bounding the central channel, viz., M1d on the inside, and M2d on the outside; basic residues are highlighted in red and acidic residues, in blue. It can be seen from the en face view that the channel widens into a substantial vestibule toward the inner surface of the fourfold, two-helix array (i.e., projecting toward the reader in Fig. 14 *B*), and is there festooned with positive charges, which should create a well for mobile anions. The corresponding longitudinal view, shown in Fig. 14, *D* and *E*, reveals the vestibule to be flask-shaped and to narrow sharply into the channel proper, which should be ~7.2 Å in diameter at the bottom of the vestibule, ~3.4 Å at the narrowest point, amid the four phenylalanine side chains, and ~5.7 Å at the outer end (*bottom*).

Although the diameter of chloride ions (~3.7 Å; Dean (40)), is larger than the narrowest part of this hypothetical structure, a likely more important physical problem is that liquid water becomes unstable in hydrophobic pores below ~6 Å diameter, according to molecular dynamic simulations (41,42). Reasonable allowance for thermal fluctuations would still leave the narrowest part of this postulated channel below that limit, so that anion currents (and water) would need to be punched through the narrow part by large gradients, even though the vestibule and upper (inner) portion of

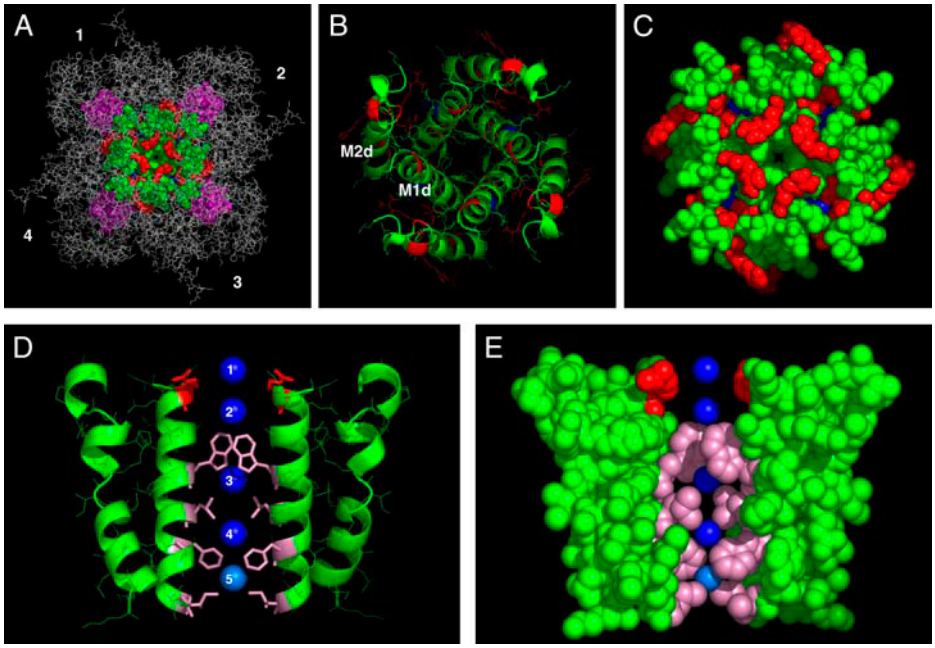

FIGURE 14 Hypothetical structure surrounding the central pore of the proposed TRK tetramer, for the (Sp)Trk1p homolog from *Schizosaccharomyces pombe*. Coordinates provided by Durell and Guy (16). (*A*) Perspective of the membrane components of the whole tetramer. White (*background*), stick-figure representation of the six transmembrane helices, M1a through M2c (refer to Fig. 1), in all four monomers. Magenta, clustered selectivity sequences of the *P*-loops, to indicate the expected location of the K^+-transport path through each monomer. (*B* and *D*) Ribbon diagrams of the interfacial transmembrane helices, M1d (*inner*) and M2d (*outer*), viewed (*B*) down the axis of the central pore from the intracellular surface of the yeast plasma membrane; and viewed (*D*) in axial (longitudinal) section from within the plane of the membrane. (*C* and *E*) Space-filling diagrams (H atoms omitted) corresponding to *B* and *D*. Drawings made with PyMol (DeLano Scientific, South San Francisco, CA). Green, neutral amino acids; red, basic amino acids; and blue, acidic amino acids. At the inner surface (*C*), charged residues would form a rather wide vestibule leading into a much narrower central pore. Both *Saccharomyces* proteins would have an additional basic residue, facing laterally, near the inner end of each M1d helix. At the outer surface (*bottom end* of *D* and *E*), neutral residues would also expand the channel, but only slightly. Blue spheres represent chloride ions in transit, without intention to designate a preferred site. Position *1*, entry diameter of the pore ~9.5 Å; position *2*, widest part of the vestibule ~15.5 Å; channel narrows abruptly below position 2, to ~7.2 Å amid the tryptophane side chains. Position *3*, chloride securely within the channel proper. Position *4*, supposed deepest penetration without voltage; below that, channel narrows to ~3.4 Å, amid the phenylalanine side chains. Position *5* (*light blue*), passage to this point and on out of the pore would require voltage-driven punchthrough. (See Appendix B for amino-acid sequences.)

the channel proper should normally be occupied by aqueous solution from the inner surface of the membrane.

This hypothetical structure for TRK-protein tetramers lends itself well, qualitatively at least, to the pH_o-dependence of the outer barrier height (E_β), and to the $[Cl^-]_i$-dependence of the inner barrier position (a_1), in the two-barrier kinetic model (Fig. 5, Eq. 2). The ring(s) of positive charge lining the vestibule near the inner surface of the membrane should create an electrostatic field with two roles: acting as a well for mobile anions, and holding the structure open. Raising free chloride concentration in the boundary solution should tend both to fill the well and to constrict it, thus shifting the energy barrier E_α toward the inner surface of the membrane. In a complementary way, changing pH_o might alter the effective stiffness or stability of the outer end of the helix array, thus reducing the electric field required to punch chloride ions (and water) through the phenylalanine ring, i.e., over E_β. Relaxation at the outer end of the structure need not reside in the passage wall per se, but in the mix of electrostatic and hydrophobic forces which hold the protein tetramer together.

Relation to other systems

This central pore hypothesis for TRK-dependent chloride currents would avoid the major problem of drastically switching affinities to permit both normal cation influx and the unexpected chloride efflux through the same channel. It also has the practical experimental advantage of focusing attention on specific amino acid residues which should be critical, and which are easy targets for both mutagenetic tests and crosslinking analysis. Such experiments on the yeast TRK proteins could shed light on a variety of other systems with adventitious chloride currents. Oligomerization is itself a commonplace phenomenon among membrane proteins, and evolution has widely appropriated the resulting central pores for critical transport functions, e.g., in F-type ATP synthases, in V-type ATPases, in transmitter-receptor proteins such as the acetylcholine receptor (AchR), in bacterial and mitochondrial porins, and in bona fide potassium channels. Thus, transport *between* protein molecules is well established, but adventitious fluxes are rarely reported, because—by definition—the necessary conditions are rarely tested. Other candidates for central-pore and/or adventitious conduction include the apparent bulk flow of water via certain aquaporins (43), gas transport via aquaporins (44), chloride currents through ABC-type transporters (45,46), and the amine- and amino-acid-activated chloride currents through transmitter transporters in neural tissue (1–4). For the latter, hard structural data on oligomerization is now beginning to emerge (10,47). Most importantly, cryoelectron microscopic pictures of the glutamate transporter EAAT3 (expressed in *Xenopus* oocytes) have demonstrated a pentameric assembly with an apparent central pore opening to the external membrane surface. This pore has also been proposed as a pathway for chloride (47).

APPENDIX A: STEADY-STATE KINETICS FOR TWO-BARRIER TRANSIT OF CHLORIDE

The simplest barrier model which can approximate the current-voltage data in Figs. 3 and 4 contains two activation steps, α and β, in series within the membrane dielectric, as depicted in Fig. 5 (*top panel*). From reaction-rate theory, chloride efflux (rightward) across each of the two barriers can be written as

$$^{o}J_\alpha = PCl_i \exp(-E_\alpha/RT)\exp(z_c a_1 F V_m/RT)$$

and

$$^{o}J_\beta = PCl_v \exp(-E_\beta/RT)\exp(z_c b_1 F V_m/RT), \qquad \text{(A1)}$$

and chloride influx (leftward) across the same barriers as

$$^{i}J_\alpha = PCl_v \exp(-E_\alpha/RT)\exp(-z_c a_2 F V_m/RT)$$

and

$$^{i}J_\beta = PCl_o \exp(-E_\beta/RT)\exp(-z_c b_2 F V_m/RT), \qquad \text{(A2)}$$

where P is an experimental scaling constant, E_α and E_β are the activation energies at the two barriers, a_1, b_1, etc. are the fractional distances which locate the barrier peaks, Cl_i and Cl_o are the intracellular and extracellular concentrations of chloride, Cl_v is a virtual concentration of chloride within the energy trough, z_c is the transported charge $= -1$ for chloride, and R, F, and T have their usual meanings. By definition, $a_1 + a_2 + b_1 + b_2 = 1$, the full thickness of the membrane dielectric.

For Eqs. A1 and A2, the electric field (potential gradient) across the membrane is assumed to be constant. Membrane voltage, normally negative inside the cell, subtracts from the energy barrier for exiting anions, and adds to the energy barrier for entering anions. As will be seen below, the assumption of steady-state transport allows four parameters to drop out of these formal relationships: the virtual concentration Cl_v, the depth of the trough, and the fractional distances a_2 and b_1. The equations can be simplified by substituting $A \equiv \exp(E_\alpha/RT)$ and $B \equiv \exp(E_\beta/RT)$ into Eqs. A1 and A2.

Transmembrane current represents the net flux of chloride, and—by the steady-state assumption—is equal across the two barriers, so that

$$I_m = z_c F(^{o}J_\alpha - {}^{i}J_\alpha) = z_c F(^{o}J_\beta - {}^{i}J_\beta), \qquad \text{(A3)}$$

from which

$$\begin{aligned}(Cl_i/A)\exp(z_c a_1 F V_m/RT) - (Cl_v/A)\exp(-z_c a_2 F V_m/RT)\\ = (Cl_v/B)\exp(z_c b_1 F V_m/RT) - (Cl_o/B)\\ \times\exp(-z_c b_2 F V_m/RT),\end{aligned} \qquad \text{(A4)}$$

and

$$Cl_v = \frac{(Cl_i/A)\exp(z_c a_1 F V_m/RT) + (Cl_o/B)\exp(-z_c b_2 F V_m/RT)}{(1/A)\exp(-z_c a_2 F V_m/RT) + (1/B)\exp(z_c b_1 F V_m/RT)}. \qquad \text{(A5)}$$

A definitive equation for the steady-state transmembrane current of chloride is then obtained by substituting this expression for Cl_v into Eqs. A1 and A2, expanding (the first half of) Eq. A3 accordingly, rearranging and canceling appropriate terms, and folding the scaling constant P into $1/A$ and $1/B$. Then, finally,

$$I_m = z_c F \frac{Cl_i \exp(z_c a_1 F V_m/RT) - Cl_o \exp(-z_c(1-a_1)F V_m/RT)}{A + B\exp(-z_c(1-a_1-b_2)F V_m/RT)}. \qquad \text{(A6)}$$

APPENDIX B: AMINO ACID SEQUENCES

The amino-acid sequences of M1d and M2d in SpTrk1p, ScTrk1p, and ScTrk2p, are shown below. Sequence similarity (identity plus conservative substitutions) between ScTrk1p and ScTrk2p is 95–100% for the two helices, and between SpTrk1p and ScTrk2p, is 74–77%.

```
                    M1d
S. pombe Trk1p:     IQRQLSHDLWYLFLGYFIITIV-774
                    . .::: ::::::: ::: :
S. cerevisiae Trk1p: LRKQLSFDLWFLFLGLFIICIC-1096
                    ::.::::::.::::::::::
S. cerevisiae Trk2p: LRRQLSFDLWYLFLGLFIICIC-762
                    M2d
S. pombe Trk1p:     KISKLVMVALQIRGRHRGLPSAL-843
                     .:::::.:. :::: :::: :
S. cerevisiae Trk1p: TLSKLVIIAMLIRGKNRGLPYSL-1166
                     ::::::::::::::.::::::.:
S. cerevisiae Trk2p: VLSKLVIIAMLIRGRNRGLPYTL-832
```

The authors are indebted, for strains, to Dr. Per Ljungdahl (Ludwig Institute, Stockholm, Sweden), and to Dr. Albert Smith (formerly in the Department of Molecular, Cellular, and Developmental Biology at Yale; now at deCode Genetics, Reykjavik); and to Dr. Esther Bashi for additional strains, for maintenance of cultures and for general assistance with experiments. We are also especially indebted to Dr. Adam Bertl (University of Karlsruhe, Germany) and Dr. H. Robert Guy (U.S. National Institutes of Health) for inspiring these experiments, and to Dr. Guy for providing the structural coordinates for the theoretical tetramer of TRK proteins. We are also grateful to Dr. Yu-Feng Zhou and Dr. Sarah Yohannan (this Department) for instruction in the use of structure-graphics software, and especially indebted to Dr. Dietrich Gradmann (University of Göttingen) and Dr. Fred Sigworth (this Department) for suggesting a barrier model. Finally, we are grateful to Dr. Guy, Dr. Louis DeFelice (Department of Pharmacology, Vanderbilt University), Dr. Dieter Oesterhelt (Max Planck Institute for Biochemistry, Munich), Dr. Hermann Bihler (Yale Department of Molecular Biophysics and Biochemistry), and Dr. S. Gwyn Ballard (this Department) for helpful comments on the manuscript.

The work was supported by Research grant No. GM-60696 to C.L.S., and by an Overseas Research Scholarship from the Japanese Ministry of Education, Culture, Sports, Science, and Technology (to T.K.).

REFERENCES

1. Sonders, M. S., and S. G. Amara. 1996. Channels in transporters. *Curr. Opin. Neurobiol.* 6:294–302.
2. Galli, A., R. D. Blakely, and L. J. DeFelice. 1996. Norepinephrine transporters have channel modes of conduction. *Proc. Natl. Acad. Sci. USA.* 93:8671–8676.
3. Arriza, J. L., S. Ellasof, M. P. Kavanaugh, and S. G. Amara. 1997. Excitatory amino acid transporter 5, a retinal glutamate transporter coupled to a chloride conductance. *Proc. Natl. Acad. Sci. USA.* 94:4155–4160.
4. Carvelli, L., P. W. McDonald, R. D. Blakeley, and L. J. DeFelice. 2004. Dopamine transporters depolarize neurons by a channel mechanism. *Proc. Natl. Acad. Sci. USA.* 101:16046–16051.
5. Su, A., S. Mager, S. L. Mayo, and H. A. Lester. 1996. A multi-substrate single-file model for ion-coupled transporters. *Biophys. J.* 70:762–777.
6. DeFelice, L. J., S. V. Adams, and D. L. Yprey. 2001. Single-file diffusion and neurotransmitter transporters: Hodgkin and Keynes model revisited. *Biosystems.* 62:57–66.
7. Ryan, R. M., A. D. Mitrovic, and R. J. Vandenberg. 2004. The chloride permeation pathway of a glutamate transporter and its proximity to the glutamate translocation pathway. *J. Biol. Chem.* 279:20742–20751.
8. Grunewald, M., and B. I. Kanner. 2000. The accessibility of a novel reentrant loop of the glutamate transporter GLT-1 is restricted by its substrate. *J. Biol. Chem.* 275:9684–9689.
9. Slotboom, J., W. N. Konings, and J. S. Lolkema. 2001. The structure of glutamate transporters shows channel-like features. *FEBS Lett.* 492:183–186.
10. Yernool, D., O. Boudker, and E. Gouax. 2004. Structure of a glutamate transporter homologue from *Pyrococcus horikoshii*. *Nature*. 431: 811–818.
11. Doyle, D. A., J. M. Cabral, R. A. Pfuetzner, A. Kuo, J. M. Gulbis, S. L. Cohen, B. T. Chait, and R. MacKinnon. 1998. The structure of the potassium channel: molecular basis of K^+ conduction and selectivity. *Science*. 280:69–76.
12. Zhou, Y., J. H. Morais-Cabral, A. Kaufman, and R. MacKinnon. 2001. Chemistry of ion coordination and hydration revealed by a K^+-channel-Fab complex at 2.0 Å resolution. *Nature*. 414:43–48.
13. Stumpe, S., A. Schlösser, M. Schleyer, and E. P. Bakker. 1996. K^+ circulation across the prokaryotic cell membrane: K^+-uptake systems. *In* Transport Processes in Eukaryotic and Prokaryotic Organisms. W.N. Konings, H.R. Kaback, and J.S. Lolkema, editors. Elsevier, Amsterdam, The Netherlands. 473–500.
14. Jan, L. Y., and Y. N. Jan. 1997. Cloned potassium channels from eukaryotes and prokaryotes. *Annu. Rev. Neurosci.* 20:91–123.
15. Durell, S. R., Y. Hao, T. Nakamura, E. P. Bakker, and H. R. Guy. 1999. Evolutionary relationship between K^+ channels and symporters. *Biophys. J.* 77:775–788.
16. Durell, S. R., and H. R. Guy. 1999. Structural models of the KtrB, TrkH, and Trk1, 2 symporters, based on the crystal structure of the KcsA K^+ channel. *Biophys. J.* 77:789–807.
17. Tholema, N., E. P. Bakker, A. Suzuki, and T. Nakamura. 1999. Change to alanine of one out of four selectivity filter glycines in KtrB causes a two orders-of-magnitude decrease in the affinities for both K^+ and Na^+ of the Na^+-dependent K^+-uptake system KtrAB from *Vibrio alginolyticus*. *FEBS Lett.* 450:217–220.
18. Kato, Y., M. Sakaguchi, Y. Mori, K. Saito, T. Nakamura, E. P. Bakker, Y. Sato, S. Goshima, and N. Uozumi. 2001. Evidence in support of a four transmembrane-pore-transmembrane topology model for the *Arabidopsis thaliana* Na^+/K^+ translocating AtHKT1 protein, a member of the superfamily of K^+ transporters. *Proc. Natl. Acad. Sci. USA.* 98:6488–6493.
19. Mäser, P., Y. Hosoo, S. Goshima, T. Horie, B. Eckelman, K. Yamada, K. Yoshida, E. P. Bakker, A. Shinmyo, S. Oiki, J. I. Schroeder, and N. Uozumi. 2002. Glycine residues in potassium channel-like selectivity filters determine potassium selectivity in four-loop-per subunit HKT transporters from plants. *Proc. Natl. Acad. Sci. USA.* 99:6428–6433.
20. Haro, R., and A. Rodriguez-Navarro. 2003. Functional analysis of the $M2_d$ helix of the TRK1 potassium transporter of *Saccharomyces cerevisiae*. *Biochim. Biophys. Acta.* 1613:1–6.
21. Zeng, G.-F., M. Pypaert, and C. L. Slayman. 2004. Epitope tagging of the yeast K^+-carrier, TRK2, demonstrates folding which is consistent with a channel-like structure. *J. Biol. Chem.* 279:3003–3013.
22. Kuroda, T., H. Bihler, E. Bashi, C. L. Slayman, and A. Rivetta. 2004. Chloride channel function in the yeast TRK-potassium transporters. *J. Membr. Biol.* 198:177–192.
23. Collins, K. D., and M. W. Wasabaugh. 1985. The Hofmeister effect and the behaviour of water at interfaces. *Q. Rev. Biophys.* 18:323–422.
24. Nicholls, P., and N. Miller. 1974. Chloride diffusion from liposomes. *Biochim. Biophys. Acta.* 336:184–198.
25. The, R., and W. Hasselbach. 1975. The action of chaotropic anions on the sarcoplasmic calcium pump. *Eur. J. Biochem.* 53:105–113.
26. Klodos, I., R. L. Post, and B. Forbush III. 1994. Kinetic heterogeneity of phosphoenzyme of Na,K-ATPase modeled by unmixed lipid phases. *J. Biol. Chem.* 269:1734–1743.

27. Hill, A. V., and L. MacPherson. 1954. The effect of nitrate, iodide and bromide on the duration of the active state in skeletal muscle. *Proc. R. Soc. Lond. B. Biol. Sci.* 143:81–102.

28. Figler, R. A., H. Omote, R. K. Nakamoto, and M. K. Al-Shawi. 2000. Use of chemical chaperones in the yeast *Saccharomyces cerevisiae* to enhance heterologous membrane protein expression: high-yield expression and purification of human P-glycoprotein. *Arch. Biochem. Biophys.* 376:34–46.

29. Bertl, A., H. Bihler, C. Kettner, and C. L. Slayman. 1998. Electrophysiology in the eukaryotic model cell *Saccharomyces cerevisiae*. *Eur. J. Physiol.* 436:999–1013.

30. Bihler, H., R. F. Gaber, C. L. Slayman, and A. Bertl. 1999. The presumed potassium carrier Trk2p in *Saccharomyces cerevisiae* determines an H^+-dependent, K^+-independent current. *FEBS Lett.* 447:115–120.

31. Blatt, M. R., and C. L. Slayman. 1983. KCl leakage from microelectrodes and its impact on the membrane parameters of a nonexcitable cell. *J. Membr. Biol.* 72:223–234.

32. Hohmann, S. 2002. Osmotic adaptation in yeast: control of the yeast osmolyte system. *Int. Rev. Cytol.* 215:149–187.

33. Hodgkin, A. L., and B. Katz. 1949. The effect of sodium ions on the electrical activity of the giant axon of the squid. *J. Physiol.* 108:37–77.

34. Marquardt, D. 1963. An algorithm for least-squares estimation of nonlinear parameters. *J. Soc. Indust. Appl. Math.* 11:431–441.

35. Bertl, A., J. Ramos, J. Ludwig, H. Lichtenberg-Frate, J. Reid, H. Bihler, F. Calero, P. Martinez, and P. O. Ljungdahl. 2003. Characterization of potassium transport in wild-type and isogenic yeast strains carrying all combinations of *trk*1, *trk*2, and *tok*1 null mutations. *Mol. Microbiol.* 47:767–780.

36. Nelson, D. J., J. Ehrenfeld, and B. Lindemann. 1978. Volume changes and potential artifacts of epithelial cells of frog skin following impalement with microelectrodes filled with 3 M KCl. *J. Membr. Biol.* 40SI:91–119.

37. Läuger, P., and G. Stark. 1970. Kinetics of carrier-mediated ion transport across lipid bilayer membranes. *Biochim. Biophys. Acta.* 211:458–466.

38. Hille, B. 1975. Ionic selectivity, saturation, and block in sodium channels. A four-barrier model. *J. Gen. Physiol.* 66:535–560.

39. Läuger, P. 1984. Thermodynamic and kinetic properties of electrogenic ion pumps. *Biochim. Biophys. Acta.* 779:307–341.

40. Dean, J. A. 1985. Lange's Handbook of Chemistry, 13th Ed. McGraw-Hill, New York. 3–122.

41. Hummer, G., J. C. Rasalah, and J. P. Noworyta. 2001. Water conduction through the hydrophobic channel of a carbon nanotube. *Nature.* 414:188–190.

42. Beckstein, O., and M. S. P. Sansom. 2003. Liquid-vapor oscillations of water in hydrophobic nanopores. *Proc. Natl. Acad. Sci. USA.* 100: 763–768.

43. Verkman, A. S., and A. K. Mitra. 2000. Structure and function of aquaporin water channels. *Am. J. Physiol.* 278:F13–F28.

44. Nakhoul, N. L., B. A. Davis, M. F. Romero, and W. F. Boron. 1998. Effect of expressing the water channel aquaporin-1 on the CO_2 permeability of *Xenopus* oocytes. *Am. J. Physiol. Cell Physiol.* 274: C543–C548.

45. Murakami, S., N. Tamura, A. Saito, T. Hirata, and A. Yamaguchi. 2004. Extramembrane central pore of multidrug exporter AcrB in *Escherichia coli* plays an important role in drug transport. *J. Biol. Chem.* 279:3743–3748.

46. Schillers, H., V. Shahin, L. Albermann, C. Schafer, and H. Oberleithner. 2004. Imaging CFTR: a tail-to-tail dimer with a central pore. *Cell. Physiol. Biochem.* 14:1–10.

47. Eskandari, S., M. Kreman, M. P. Kavanaugh, E. M. Wright, and G. A. Zampighi. 2000. Pentameric assembly of a neuronal glutamate transporter. *Proc. Natl. Acad. Sci. USA.* 97:8641–8646.